British Geological Survey
Natural Environment Research Council

Saline Aquifer CO2 Storage Phase 2 (SACS2)

Work Area 5 (Geophysics) – Gravity monitoring of the CO_2 bubble

BGS Commissioned Report CR/01/063N

Open

This page is blank

Saline Aquifer CO_2 Storage: A Demonstration Project at the Sleipner Field

Work Area 5 (Geophysics) – Gravity modelling of the CO_2 bubble

BGS Commissioned Report CR/01/063N (Open)

Contract Number:	T-124.167-02
Contractor:	Den Norsk Stats Ojleselskap A.S.
Date:	31/03/01
Authors:	J.P. Williamson, R.A. Chadwick, W.J. Rowley, (BGS) O. Eiken (Statoil)

British Geological Survey
March 2001

This page is blank

Contents **Page**

Executive Summary 3
1. Introduction 5
2. Geometry of the CO_2 bubble in October 1999 5
3. Density estimates 6
    3.1 Density of CO_2 in the subsurface 6
    3.2 Effective density contrast 6
    3.3 Effective CO_2 saturation within the bubble envelope 7
4. Gravity modelling 8
    4.1 Gravity effect of the *in situ* CO_2 bubble 1999 (2.28 MT CO_2) 8
    4.2 Gravity effect of the *in situ* CO_2 bubble 2001 (~4 MT CO_2) 8
    4.3 CO_2 migration scenario 1 – vertical migration into caprock 9
    4.4 CO_2 migration scenario 2 – single layer lateral migration beneath caprock 10
    4.5 Direct measurement of mass deficit due to CO_2 12
5. Gravimetric survey sensitivity and logistics 12
6. Conclusions and recommendations 13
7. References 14

Tables

Table 1 Geometrical properties of the GOCAD 3-D model of the bubble envelope

Table 2 Pressure – temperature – density model for the Utsira reservoir, overburden and injected CO_2

Table 3 Effective density contrasts for the GOCAD model and for the cylindrical approximation, for selected values of CO_2 density

Text Figures

Figure 1 Image of the CO_2 bubble on the 1999 time-lapse 'difference' data (1999 signal minus 1994 signal). Surface and injection locations of injection well are accurate, but intermediate trajectory is schematic.

Figure 2 Timeslice from the 1999 time-lapse difference data at 950 ms showing relatively simple geometry of the bubble amplitude anomaly. Yellow polygons denote the interpreted outer edge of the CO_2 bubble.

Figure 3 1999 time-lapse difference data showing complexity in the CO_2 bubble a) time-slice at 920 ms showing line of cross-section. Yellow polygons denote the interpreted outer edge of the CO_2 bubble envelope. b) section illustrating bubble geometry (arrow marks level of time-slice).

Figure 4 a) Relationship of the injection platform (N15/9-A16) and the velocity control well (N15/9-13) to the injection point, and seismic profile through the wells and the CO_2 bubble b) time-depth relationship for well N15/9-13 with modification for velocity push-down (red dashed line).

Figure 5 a) Stack plot of the time-lapse difference amplitude anomalies digitised on successive time-slices. Heavy line denotes best-fit ellipse used as plan section of cylinder approximation. b) 3-D image of the bubble envelope, together with section through the difference time-slice.

Figure 6 Temperature-depth and density-depth profiles through the Utsira Sand and overburden.

Figure 7 Effective density contrast of the bubble envelope volume as a function of CO_2 density.

Figure 8 Peak gravity anomaly October 1999 due to the GOCAD model computed on the sea surface (solid symbols) and the sea bed (open symbols) as a function of CO_2 density.

Figure 9 Peak gravity anomaly projected to 2001 (~ 4 MT CO_2) due to the GOCAD model computed on the sea surface (solid symbols) and the sea bed (open symbols) as a function of CO_2 density.

Figure 10 Modelled gravity anomaly for cylindrical approximation model, with top at 375 m depth and base at 600 m depth (ρ_{CO2} = 150 kgm^{-3}). Round marker denotes subsurface location of injection point.

Figure 11 (a) Thickness of CO_2 saturated rock column after 21 MT of CO_2 injected, assuming CO_2 is trapped in structural closures at top Utsira Sand. Reservoir porosity = 0.3; net/gross = 0.85. From Zweigel et al. 2000. (b) Perspective view of the CO_2 accumulation viewed from the SW (vertical exaggeration x75).

Figure 12 Modelled gravity anomalies (μGal) for 3 x 10^7 m^3 of injected CO_2 assuming lateral migration beneath caprock as a single thin layer of CO_2 (a) 21 MT at density of 700 kgm^3 (b) 10.5 MT at density of 350 kgm^3.

Executive Summary

A principal aim of the SACS project is to monitor the injected CO_2 by geophysical methods and to develop a robust and repeatable monitoring and verification methodology for future CO_2 sequestration operations. This report evaluates the applicability of microgravity surveys as a means of monitoring the future subsurface distribution and migration of the Sleipner CO_2 bubble.

Time-lapse seismic data acquired in 1999, after 2.3 MT of CO_2 injection, show an exceptionally clear image of the CO_2 bubble, characterised by very high reflection amplitudes. The outer envelope of the amplitude anomaly roughly defines an elliptical cylindrical 'bubble envelope', ~ 225 m high, with a major axis of ~ 1500 m oriented NNE and a minor axis of ~ 600 m.

Gravity modelling was based on a number of scenarios. Two '*in situ*' scenarios assume that the CO_2 is entirely contained within the bubble envelope. The 1999 and 2001 *in situ* models assume respectively that 2.3 MT and 4MT of CO_2 are contained within the envelope. Two migration scenarios are also modelled. The first assumes that 2.3MT of CO_2 migrate vertically upwards into the overlying caprock succession to between depths of 375 and 600 m. The second migration model looks further ahead to the situation where 3×10^7 m^3 (~ 10.5 – 21.0 MT depending on the density) of CO_2 have been injected, and migrate laterally beneath the caprock at the top of the reservoir.

Results depend strongly on the assumed density of the injected CO_2 at reservoir conditions, which is subject to significant uncertainty. Only one, poorly-constrained, reservoir temperature measurement of 37 ° C is available. A density-depth profile based on this suggests that the density of CO_2 in the reservoir is ~ 700 kgm^{-3}. However the possibility of significantly lower densities cannot be discounted and modelling also includes a lower density case of 350 kgm^{-3}.

The 1999 and 2001 *in situ* cases produce anomalies which would be barely detectable if the higher density of CO_2 is assumed. With the lower density however anomalies should be readily detectable with a modern seabed gravimeter. The vertical migration scenario indicates that large-scale vertical migration into the caprock, to depths where densities would be unequivocally lower, would be readily detected. The lateral migration scenario, whereby a single thin layer of CO_2 migrates beneath the top reservoir seal, produces small anomalies which may be locally detectable but with insufficient resolution to enable effective migration mapping. However if lateral migration is via several layers, beneath intra-reservoir shales, then anomalies should be more usefully measurable.

Obtaining time-lapse gravimeter readings directly above the bubble would appear to offer the best chance of obtaining useful information. Coupled with geometric information provided by the time-lapse seismic data, the gravity should be able to discriminate between the low and high CO_2 density scenarios. This would provide important constraints on future reservoir modelling and also the volume estimates based on the seismic velocity pushdown effect. Related to this, gravity data would offer the potential to provide independent verification of the amount of CO_2

sequestered. In addition gravimetric surveys above the bubble could provide an effective ‘early warning’ of major caprock breaching.

1. Introduction

This report describes the results of Task 5.1 in SACS2 Work Area 5 (Geophysics). The aim of the Task is to evaluate the applicability of microgravity surveys as a means of monitoring the future subsurface distribution and migration of the Sleipner CO_2 bubble.

2. Geometry of the CO2 bubble in October 1999

The geometry of the CO_2 bubble in this study is based upon the image obtained by the 1999 time-lapse seismic survey which very clearly shows enhanced reflectivity associated with that volume of the Utsira reservoir occupied by CO_2 (Figure 1).

The 3-D geometry of the CO_2 bubble was defined by interpreting the amplitude anomaly on the time-lapse 'difference' data on a series of time-slices. The top time-slice, at 854 ms defines the topmost detectable amplitude anomaly. Subsequent time-slices were interpreted at 10 ms intervals to the basal time slice at 1104 ms, corresponding to the elevation of the injection point. Some of the interpretation was straightforward where the bubble was structurally simple (Figure 2). In other places the bubble was structurally more complex, with the apparent development of 'chimneys' of CO_2 (Figure 3), here precise interpretation of the bubble was less certain. The interpreted bubble morphology is likely to represent the 'outer envelope' of the space occupied by the CO_2, due to the presence of spurious events deeper in the bubble image. These occur for two reasons. Firstly, there is evidence that the data is affected by seabed multiples, meaning that some of the signal deeper in the bubble is likely to be spurious. Second, is the fact that the difference data register the effects of velocity pushdown within the bubble as well as changes in reflection amplitude. Thus, events beneath CO_2 accumulations are displaced in travel-time, even if their amplitude is unchanged. This generates spurious signal within the difference image data (Figure 1). To minimise the effects of this, the difference data time-slices were interpreted in conjunction with the observed 1999 seismic data and obviously spurious signals were ignored. The precise distribution of CO_2 within the bubble is the subject of more detailed studies in other Tasks, and is not critical to this study which just requires a general description of the total volume occupied by the CO_2.

A depth image of the CO_2 bubble was obtained by depth-converting each time-slice using a velocity model based on the velocity survey from Norwegian well 15/9-13, which lies about 870 m WSW of the injection point (Figure 4a). In carrying out the depth conversion it was necessary to correct for the effects of velocity 'pushdown' within the bubble. The amount of pushdown varies laterally across the bubble, depending on the amount of CO_2 in the column (Rob Arts personal communication), and is by far the greatest in the central part. For the purposes of depth conversion a value of +30 ms at the base of the bubble, decreasing linearly to zero at the top of the bubble, was used to modify the travel-time – depth relationship (Figure 4 b).

The interpreted time slices, corresponding to depths between the top (854ms, 787m bsl) and base (1104ms, 1012m bsl) of the bubble were digitised. A plan view of the digitised time-slice data (Figure 5a) shows the form of the bubble to be strongly

anisotropic, with a maximum horizontal dimension of approximately 2km. Each digitised depth slice was imported into GOCAD as a closed curve and filtered to reduce the point spacing to 50m. A triangulated surface representing the bubble outer envelope was then constructed from the curves, taking care to ensure that the resulting surface was closed (Table 1, Figure 5b). This 3-D surface is taken to define the volume within which all of the injected CO_2 is situated (at the time of the 1999 time-lapse survey). N.B. The actual volume of CO_2 saturated rock is likely to be considerably smaller than this.

3. Density estimates

3.1 Density of CO_2 in the subsurface

The density of CO_2 in the subsurface is strongly dependent on pressure and temperature. Within the bubble, CO_2 is close to its critical point, and its density is particularly sensitive to changes in the ambient conditions. Information on the temperature within the Utsira Reservoir is currently limited to a single downhole measurement of 37 °C at a depth of 1058 m below sea level (Erik Lindberg personal communication). A simple thermal model was constructed based upon this measurement, assuming a predominantly argillaceous overburden to the Utsira reservoir (Table 1). Pressures and temperatures were computed for a range of depths, from seabed down to the Utsira reservoir, with the density of the CO_2 calculated for each P-T pair (Sintef in-house algorithm). A plot of temperature and CO_2 density against depth, based on this single temperature measurement, (Figure 6) shows density to have a strong depth dependence. At depths greater than about 700 m the CO_2 would exist as a supercritical fluid with a density of ~ 700 kg m^{-3}, whereas as depths less than about 600 m it exists in the gaseous state with a much lower density, typically less than ~ 200 kgm^{-3}.

It must be stressed however that these figures are based on a single temperature measurement in the Utsira reservoir, which is subject to considerable uncertainty (typically 2 – 5 °C). If the temperature of 37°C is an underestimate, then the possibility remains that the CO_2 is significantly less dense than the predicted in Table 1. Analysis of the velocity pushdown beneath the CO_2 bubble (Rob Arts personal communication) is consistent with a lower CO_2 density (about 360 kg m^{-3}). The following modelling allows for both high and low density situations.

3.2 Effective density contrast

The bubble forms by injected CO_2 displacing water from the pore space, however the precise distribution of CO_2 within the bubble envelope is not known. In order to compute the gravity anomaly of the bubble it is necessary to know the effective density contrast Dr between the bubble and the surrounding rock. This is computed as follows:

The total volume of the bubble envelope is V

Injected volume of CO_2 $\quad V_{CO_2} = \frac{M_{CO_2}}{r_{CO_2}}$

Expelled volume of water $\quad V_w = \frac{M_w}{r_w}$

The mass change DM within V is

$$\Delta M = M_{CO_2} - M_w = M_{CO_2} - \frac{r_w}{r_{CO_2}} M_{CO_2} = M_{CO_2}\left(1 - \frac{r_w}{r_{CO_2}}\right)$$

Assuming uniform distribution of this mass deficit within the bubble volume V, the effective density contrast Dr with the host rock is

$$\Delta r = \frac{\Delta M}{V} = \frac{M_{CO_2}}{V}\left(1 - \frac{r_w}{r_{CO_2}}\right)$$

Using:

M_{CO2} $= 2.286 \times 10^9$ kg
V $= 1.21 \times 10^8$ m^3 (GOCAD model volume)
r_w $= 1030$ kg m^{-3}

$$\Delta r = 18.89 \times \left(1 - \frac{1030}{r_{CO_2}}\right) \text{ kg m}^{-3}$$

The relationship between effective density contrast and CO_2 density, for the GOCAD model, is displayed graphically in Figure 7.

3.3 Effective CO_2 saturation within the bubble

The volume occupied by pure CO_2 within the reservoir is given by:

$$V_{CO_2} = \frac{M_{CO_2}}{r_{CO_2}}$$

and also by:

$$V_{CO_2} = Vf(1 - V_{sh})S_{CO_2}$$

Where V is the volume of the bubble envelope, f is the reservoir porosity, V_{sh} is the shale volume and S_{CO_2} is the average CO_2 saturation within the bubble envelope

Equating these two expressions, we can compute the CO_2 saturation within the measured volume.

$$S_{CO_2} = \frac{M_{CO_2}}{f(1-V_{sh})Vr_{CO_2}}$$

Plugging some figures into this (assume f = 0.35, V_{sh} = 0.15), for the GOCAD model:

$$S_{CO_2} = \frac{2.286\times10^9}{0.35\times(1-0.15)\times1.21\times10^8 \times r_{CO_2}}$$

For the high and low CO_2 density options we get:

r_{CO_2} (kg.m^{-3})	S_{CO_2}
700	0.091
350	0.181

These figures indicate a theoretical average saturation assuming the CO_2 were distributed uniformly throughout the bubble. In reality the CO_2 accumulates in discrete layers of much higher saturation, occupying only a small fraction of the total bubble volume.

4. Gravity modelling

4.1 Gravity effect of the in situ CO_2 bubble 1999 (2.28 MT CO_2)

The gravity anomaly of the GOCAD geometrical model was computed for a range of CO_2 densities, using the method of Okabe (1979), on a 4×4 km grid centred on the bubble, using a grid spacing of 100m. Calculations were made at the sea surface and on the seabed, assumed to be at a depth of 81m. The peak amplitude of the computed anomaly varies as a function of CO_2 density (Figure 8). For the higher CO_2 density of 700 kgm^{-3} (supercritical CO_2) the peak gravity anomaly would be less than -10 μGal. For the lower density situation, 350 kgm^{-3}, the peak gravity anomaly would be around -30 μGal. These values are well below the sensitivity of a shipborne gravity meter (0.3-1 mGal, 300 - 1000 μGal), but a more recently developed seabed gravimeter (Eiken et al. 2000) has a sensitivity of about 10-20 μGal. This is probably insufficiently accurate to detect the gravity anomaly as of 1999, if CO_2 density were around 700 kgm^{-3}, but possibly able to detect the anomaly if the CO_2 density were around 350 kgm^{-3}.

4.2 Gravity effect of the in situ CO_2 bubble 2001 (~4 MT CO_2)

Looking ahead to the 2001 seismic time-lapse survey, perhaps the simplest situation would be that the CO_2 bubble has continued to fill but without significant lateral migration out of the 1999 bubble envelope (by accumulation beneath the intra-

reservoir shale layers and beneath the caprock). In other words the bubble volume has remained constant but the mean saturation of CO_2 within the bubble envelope has increased,. The gravity effect of this was calculated as above (Figure 9).

As above, the calculated peak amplitude of the resulting anomaly varies as a function of CO_2 density (Figure 9). For the higher CO_2 density of 700 kgm^{-3} (supercritical CO_2) the peak gravity anomaly would be about -18 μGal. For the lower density situation, 350 kgm^{-3}, the peak gravity anomaly would be nearly -60 μGal. The seabed gravimeter would possibly be able to just detect the gravity anomaly of 2001, if CO_2 density were around 700 kgm^{-3}, and should certainly be able to detect the anomaly if the CO_2 density were around 350 kgm^{-3}. The difference in peak anomaly values between the high and low density cases is roughly 45 μGal. Deployment of a gravity survey above the bubble, coupled with geometrical information from the time-lapse seismic data, should provide the means of discriminating between the high and low CO_2 density limits. Such information would be invaluable in calibrating the CO_2 volume analysis based on Gassmann modelling of the seismic velocity 'pushdown'.

Further increase in CO_2 amounts within the *in situ* bubble in the years beyond 2001, will increase the gravity contrast, in a manner similar to, but with larger changes than the modelled cases.

4.3 Migration scenario 1 – vertical migration into caprock

The simplest migration scenario assumes that the caprock does not form an effective seal, but instead allows the CO_2 bubble to migrate vertically upward from its current position. In order to simulate this a simplification of the 3-D GOCAD model was developed. Using the best-fit ellipse of the interpreted time-slice amplitude anomalies (Figure 5a), a cylindrical approximation of the GOCAD model was generated (Table 3). The cylinder is elliptical in plan, with a height of 225 m, identical to that of the GOCAD model. Its volume however, is larger, such that $V_{cyl} = 1.92479 \times 10^8$ m^3.

Using the previous notation, the effective density contrast of the cylindrical approximation model can be written:

$$\Delta r_{cyl} = \frac{M_{CO2}}{V_{cyl}} = 11.88 \times \left(1 - \frac{r_w}{r_{CO_2}} \right)$$

Thus, for a given CO_2 density, the effective density contrast of the cylindrical model is lower than that of the GOCAD model (by the inverse ratio of the model volumes). Some values of effective density contrast are given in Table 3.

For the purpose of modelling it is assumed that the bubble envelope is simply translated vertically upwards, while maintaining overall geometrical form. Assuming the geotherm based on the available temperature measurement, at depths less than about 600m (Figure 6), CO_2 would pass into a gaseous phase with a much lower density than in its supercritical fluid state (this would be accompanied by an expansion of the CO_2 which would thereby expel more pore-water from within the

bubble envelope volume). The 'migration cylinder' was placed so as to reflect this phase change, with its base at a depth of 600 m and its top at 375 m. The cylinder was modelled as a triangular faceted body with 90 segments, giving a total of 360 facets. A density contrast of -60.95 kgm^{-3} was used, corresponding to a CO_2 density of 150 kgm^{-3} (Table 3), and gravity values were calculated on the sea floor on a 50 m regular grid. The calculated gravity anomaly (Figure 10), has an overall elliptical form, corresponding to the plan geometry of the cylinder, with a peak value of -235 μGal.

Whether such a bulk upward translation of the bubble is strictly geologically feasible is open to question. Clearly the porosity/permeability characteristics of the caprock would be radically different from the Utsira reservoir and the distribution of CO_2 within such a caprock volume would likely be severely heterogeneous. Nevertheless, the mean saturation values in the reservoir are currently very low, so caprock porosity may be able to accommodate the CO_2 within a volume which geometrically, can be adequately simulated by a simple upward translation of the bubble.

This computed anomaly for upward migration would still not be detectable by conventional shipborne measurements, but would be detectable by seafloor technology as described above.

4.4 Migration scenario 2 – single layer lateral migration beneath caprock

An alternative, perhaps more realistic scenario, is that the CO_2 is trapped as a single layer, at, or close to the base of the caprock, migrating laterally under buoyancy forces, to fill structural traps at the top of the reservoir. Zweigel et al. (2000) modelled various migration scenarios, assuming 3×10^7 m^3 of injected CO_2, a reservoir porosity of 30% and a net sand ratio of 0.85. One of their preferred models (U-3), involves westward migration at the top of the Utsira Sand. The distribution of CO_2 after completion of migration i.e. with the CO_2 contained fully within structural traps at the top of the reservoir, is illustrated in Figure 11.

In this scenario the total volume of injected CO_2 is 3.0×10^7 m^3. Assuming a density of 700 kgm^{-3}, the total mass injected would be 2.1×10^{10} kg (comparable with the final projected amount of CO_2 on completion of injection). If the lower CO_2 density of 350 kgm^{-3} were assumed, the total mass injected would be 1.05×10^{10} kg.

The colour shaded plot of CO_2 thicknesses (Figure 11a) was contoured by hand. The thickness contours were digitised and converted to depth, by placing them on a flat base at depth 787 m. The resulting depth values were gridded using a minimum-tension algorithm onto a uniform grid with 25m inter-node spacing. Figure 10b illustrates the model: the shaded region has X and Y extents of 14km and 10km respectively, while the maximum height of the CO_2 column is 25m. The total volume of rock filled with CO_2 was calculated to be 1.328×10^8 m^3 (using the program GRDVOLUME, part of the GMT package, Wessel & Smith, 1991).

Unlike the previous models, in this scenario the CO_2 saturation is, by definition, 100%. The total pore volume within the bubble volume *V* is:

$$V_{pore} = f(1-V_{sh})V$$

where f is porosity and V_{sh} is the shale factor.

Before injection, this volume was totally filled with water, so the mass change as a consequence of the injection of CO_2 is:

$$\Delta M = f(1-V_{sh})V(r_{CO_2} - r_w)$$

and the effective density contrast is therefore:

$$\Delta r = f(1-V_{sh})(r_{CO_2} - r_w)$$

Using f = 0.30, V_{sh} = 0.15, r_{CO2} = 700 kgm^{-3} and r_w = 1030 kgm^{-3} (following Zweigel et al. 2000) the density contrast is computed as

Dr = - 84.15 kgm^{-3}

For r_{CO2} = 350 kgm^{-3} the density contrast is computed as

Dr = - 173.40 kgm^{-3}.

The gridded model can be checked by comparing the predicted volume of CO_2 with the specified injected volume. The gridded model predicts a CO_2 volume of $0.3 \times 0.85 \times 1.328 \times 10^8$ m^3 = 3.39×10^7 m^3. Since the injected volume was specified as 3.0×10^7 m^3 it is clear that the gridded model overestimates the volume by approximately 13%. This is principally due to inaccuracy in converting the colour-shaded thickness image into a simplified contour map and is readily corrected (below).

The gravity anomaly of the gridded model was computed using program GM3D (Rollin, 1988), which calculates the gravity anomaly of a surface defined by a grid using a vertical prism method. To reduce computation times, the 25 m grid used for volume estimation was resampled to a spacing of 100 m for the purpose of gravity calculation. Density contrasts of - 84.15 kgm^{-3} and – 173.40 kgm^{-3} were used, corresponding to CO_2 densities of 700 kgm^{-3} and 350 kgm^{-3} respectively. The resulting computed anomalies were scaled by a factor of 0.886 to correct for the volume overestimate in the model (see above). The gravity anomalies resulting from the model (Figures 12a and 12b) show peak anomaly values of about -13 μGal for the high density scenario and – 25 μGal for the lower density scenario.

For the higher density CO_2 case the anomalies would not be reliably detectable. For the lower density case the anomalies would be marginally detectable with current seabed gravimeters. It is worth noting also that the lower density case involves injected only 10.5 MT of CO_2, so the final injection scenario would be expected to provide significantly larger anomalies.

Nevertheless, the conclusions arising from this migration scenario are that the lateral migration of CO_2 in a single thin layer much reduces the gravity signature compared

to when the CO_2 is concentrated in a thick bubble. Note however, that if the CO_2 were to migrate laterally beneath several intra-reservoir shales, as well as beneath the caprock, then its gravity signature would be increased commensurately, probably to measurably useful levels.

4.5 Direct measurement of mass deficit due to CO_2

As well as providing information on migration behaviour, the gravity data may also be used to provide an independent estimate of the mass deficit associated with injection. Application of Gauss' theorem to the residual gravity anomaly allows the unique estimation of the excess (or deficit) mass giving rise to the anomaly as:

$$\Delta M = \frac{1}{2pG} \int_{-\infty}^{+\infty} \int_{-\infty}^{+\infty} g(x,y)dxdy$$

Where ΔM is the excess mass, G is the gravitational constant and $g(x,y)$ is the residual gravity anomaly. The double integral in the above equation can be approximated by computing the 'volume' enclosed between the grid of gravity anomalies and the zero plane. For this technique to be viable, the gravity anomaly has to be of sufficient size for its morphology to be reasonably accurately mapped. With a suitable network of gravity stations this may be possible for amounts of CO_2 less than 10 MT, distributed within a relatively thick bubble envelope.

5. Gravimetric survey sensitivity and logistics

Shiborne gravity meters typically have an accuracy of 0.3-1mGal (300-1000 μGal), so the computed anomalies as described above would probably not be detectable by shipborne gravity measurements. An alternative possibility is to measure gravity on the seafloor. A newly developed instrument and measurement setup for this purpose (Eiken et al. SEG Annual Meeting 2000) has acquired seafloor gravity readings in the North Sea with an uncertainty (standard deviation) of 20-30 μGal. This has later been improved to 18-20 μGal for a single measurement, and improved further by repeat measurements (unpublished results, Statoil).

Seafloor measurements may be taken with an ROV-carried instrument on pre-deployed seafloor benchmarks, or they may be made by just lowering an instrument from a ship and onto the seafloor. The former is preferable because the elevation of the gravimeter will be uniform and local terrain (bathymetry) effects will be unchanged. In the latter case, a few metres change in position between the time-lapse measurements may be tolerable, but any height changes caused by this needs to be compensated for. Precise depth measurements can be done by measuring relative pressure, with an accuracy of 1-2 cm (Eiken et al. 2000), causing an uncertainty in gravity of only 2-4 μGal.

The cost of seafloor surveys may be divided into:

i) mobilisation and rent of equipment

ii) ship time
iii) data analysis

It may be possible to survey 10-20 sites per day. Frequent repetition of readings will improve accuracy. A typical survey of 50-200 locations may take 1-3 weeks. Typical North Sea ship costs are 10000 Euro/day without ROV and 30-40000 Euro/day with ROV. The other expenses add to this. However, if a survey could be combined with other gravity monitoring surveys in the North Sea, mobilisation costs would be reduced significantly.

One viable survey outline would be to acquire data along three or four lines crossing the dome above the injection point, and those north and south of it, and let the seismic data show the 3-D structure of the injected CO_2. For instance, about 10 km of profiles, with a station spacing of 200-400 m, would require 25-50 stations. Several repeats of each station would then be affordable, possibly pushing the accuracy below 10 μGal.

6. Conclusions and recommendations

The possibility of monitoring the behaviour of injected CO_2 with repeated gravity measurements is strongly dependent on CO_2 density and subsurface distribution. In general terms the size of the gravity change gives information on densities, while the spatial variation in gravity gives information on lateral CO_2 distribution. The weakest aspect of the gravity data is in giving information on depth to the CO_2 accumulation.

Low densities and a concentrated CO_2 bubble will give the largest gravity changes. Under such favourable circumstances and assuming a sensitivity of 10-20 μGal, this may give a signal change which is detectable after one to two years' injection at Sleipner. On the other hand, if densities are greater than 600 kgm^{-3} several tons of injected CO_2 are required to generate a measurable response,.

Obtaining time-lapse gravimeter readings directly above the bubble would appear to offer the best chance of obtaining useful information. Coupled with geometric information provided by the time-lapse seismic data, the gravity should be able to discriminate between the low and high CO_2 density scenarios. This would provide important constraints on future reservoir modelling and also the Gassmann analysis of the seismic velocity pushdown effect. Related to this, from Gauss's Law the gravity data would offer the potential to provide independent verification of the amount of CO_2 sequestered.

To investigate this further, seafloor gravity data could be acquired on a number of locations above the main dome which is currently filling up, and the adjacent domes as well. A first survey should then be done as soon as possible, followed by a repeat survey 2-5 years later. Such a project must be rated against other investigations of the CO_2 bubble.

In more general terms, the gravity anomalies discussed above are well within the range of detectability for land gravity meters, where accuracy as good as 5-10 μGal can be achieved if great care is taken. Land gravimetry is inexpensive and may well prove a useful tool for monitoring future onshore CO_2 injection operations.

7. References

Eiken. O., Zumberge, M. and Sasagawa, G., 2000, Gravity monitoring of offshore gas reservoirs. SEG annual meeting abstract.

Okabe, M. 1979. Analytical expressions for gravity anomalies due to homogeneous polyhedral bodies and translations to magnetic anomalies. Geophysics. Vol 44, p730-741.

Rollin, K. E., 1988. GM3D: Forward and iterative 3-D gravity and magnetic modelling using vertical square prisms. British Geological Survey, Technical Report WK/88/17.

Wessel, P. and Smith, W. H. F., 1991. Free software helps map and display data. EOS trans. AGU, 72, 441 & 445-446.

Zweigel, P., Hamborg, M., Arts, R., Lothe, A.E., Sylta, O., Tommeras, A. & Causse, E. 2000. Simulation of injected CO2 in the Sleipner case by means of a secondary migration modelling tool – a contribution to the Saline Aquifer CO2 Storage project (SACS). Sintef report 23.4285.00/01/00 (confidential).

Number of vertices	2568
Number of triangles	5128
Closed Volume	1.20756×10^8 m^3
Surface area	5.73017×10^6 m^2

Table 1 Geometrical properties of the 3-D model of the bubble envelope

SLEIPNER TEMPERATURE - PRESSURE MODEL

Model parameters:

seabed	80 m depth	7 degrees C
temperature measurement	1058 m depth	37 degrees C
heatflow	45.88 mWm^{-2}	

Utsira overburden = 80% shale 20% sand (depth-dependent thermal conductivity)
Utsira reservoir = 100 % sand (depth-dependent thermal conductivity)

depth below seabed (m)	depth below sea-level (m)	temperature (deg C)	hydrostatic pressure (bar)	CO_2 density (kgm^{-3})	comments
	0		1.0133		
0	80	7.00	9.1	18.24	seabed
20	100	7.73	11.1	22.55	
120	200	11.31	21.2	45.76	
220	300	14.80	31.3	72.53	
320	400	18.20	41.4	104.57	
420	500	21.49	51.5	145.64	
520	600	24.70	61.6	208.00	
620	700	27.81	71.7	695.06	
720	800	30.84	81.8	695.89	Top Utsira Sand
820	900	33.29	92.0	704.75	
920	1000	35.66	102.1	711.49	
978	1058	37.00	107.9	714.89	temperature measurement point
1020	1100	37.95	112.2	717.21	Base Utsira Sand

Table 2 Pressure – temperature – density model for the Utsira reservoir, overburden and injected CO_2

r_{CO2} ($kg.m^{-3}$)	Dr_{Gocad} ($kg.m^{-3}$)	Dr_{cyl} ($kg.m^{-3}$)
150	-110.85	-69.67
200	-78.41	-49.29
500	-20.03	-12.58
700	-8.90	-5.60

Table 3 Effective density contrasts for the GOCAD model and for the cylindrical approximation, for selected values of CO_2 density

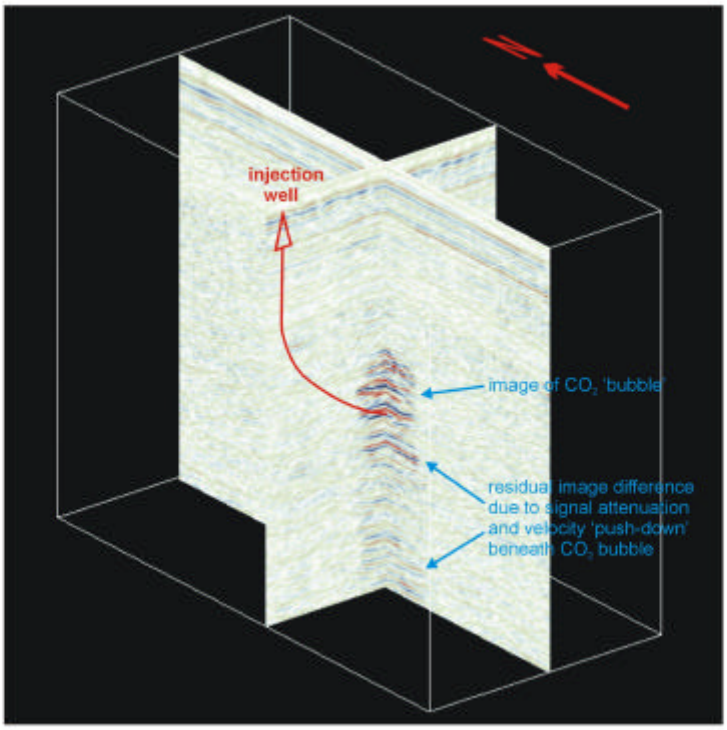

Figure 1 Image of the CO_2 bubble on the 1999 time-lapse 'difference' data (1999 signal minus 1994 signal). Surface and injection locations of injection well are accurate, but intermediate trajectory is schematic.

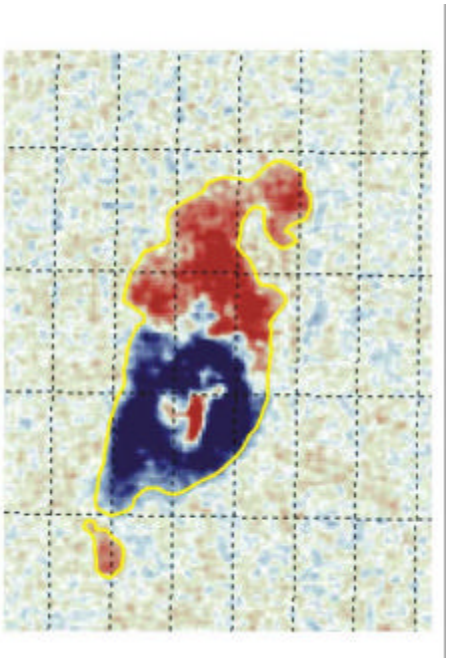

Figure 2 Timeslice from the 1999 time-lapse difference data at 950 ms showing relatively simple geometry of the bubble amplitude anomaly. Yellow polygons denote the interpreted outer edge of the CO_2 bubble.

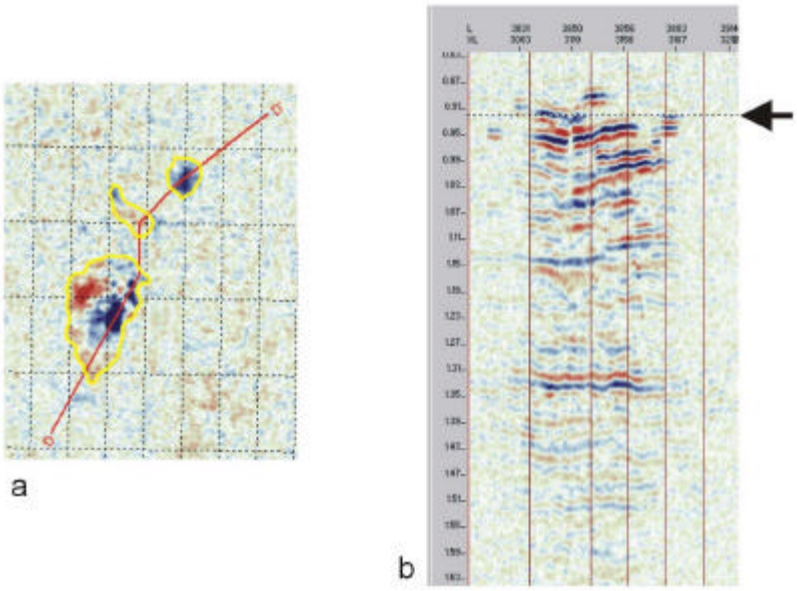

Figure 3 1999 time-lapse difference data showing complexity in the CO_2 bubble a) time-slice at 920 ms showing line of cross-section. Yellow polygons denote the interpreted outer edge of the CO_2 bubble envelope. b) section illustrating bubble geometry (arrow marks level of time-slice).

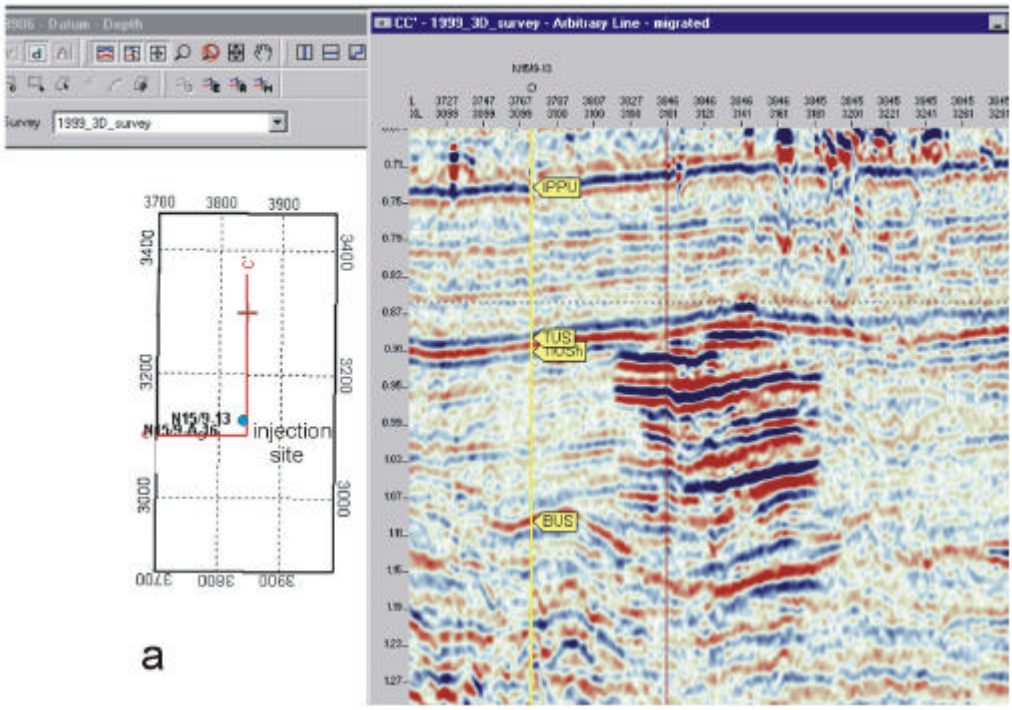

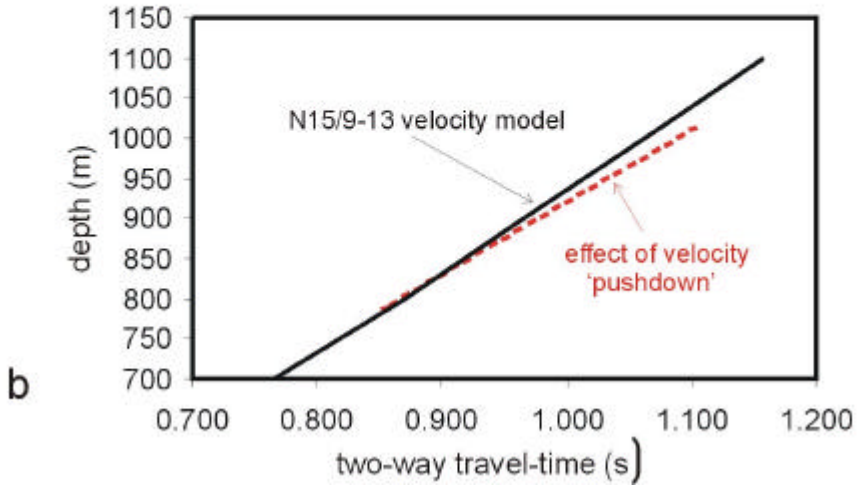

Figure 4 a) Relationship of the injection platform (N15/9-A16) and the velocity control well (N15/9-13) to the injection point, and seismic profile through the wells and the CO2 cloud b) time-depth relationship for well N15/9-13 with modification for velocity push-down (red dashed line).

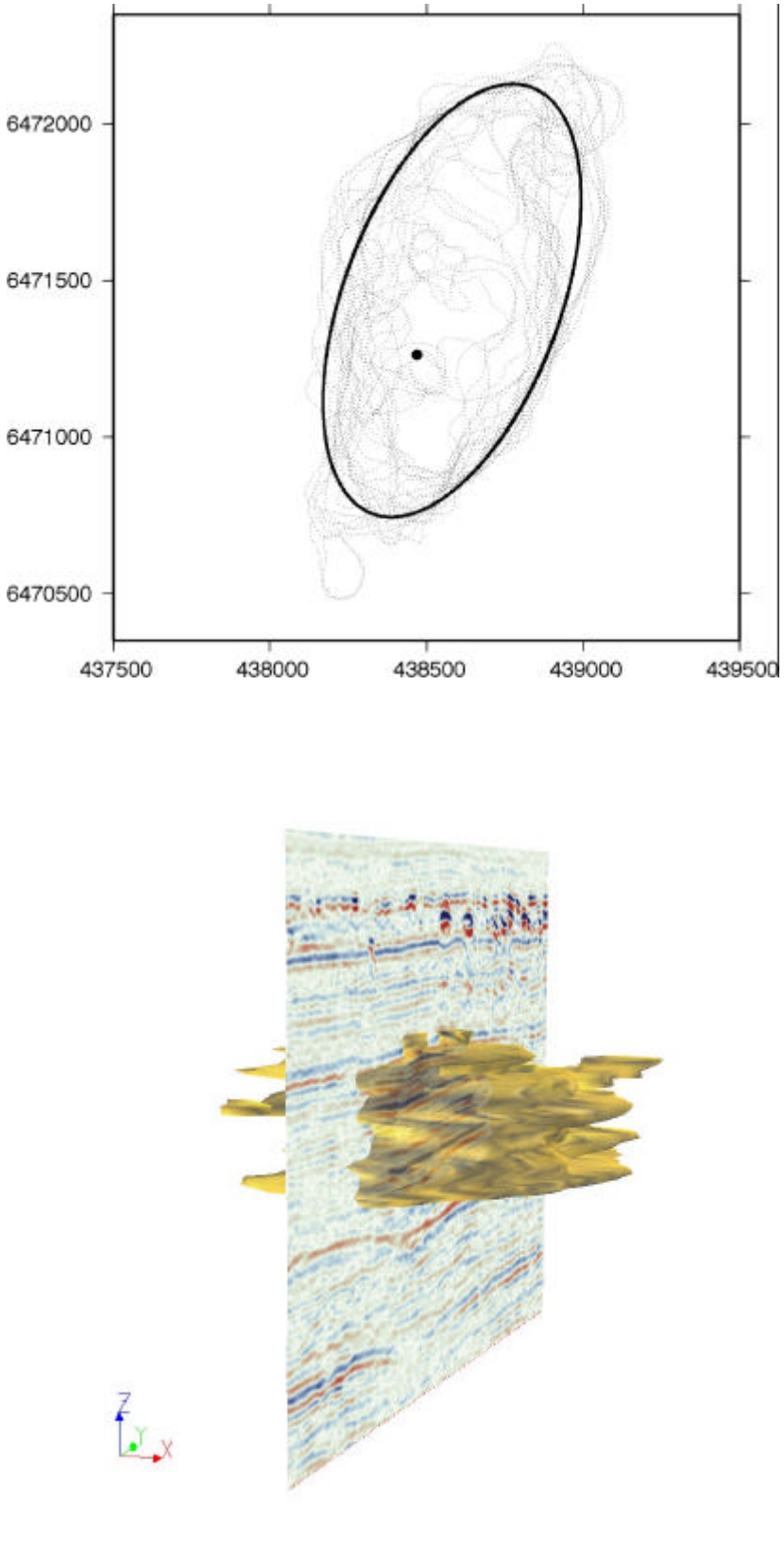

Figure 5 a) Stack plot of the time-lapse difference amplitude anomalies digitised on successive time-slices. Injection point denoted. Heavy line denotes best-fit ellipse used as plan section of cylinder approximation. b) 3-D image of the bubble envelope, together with section through the difference time-slice

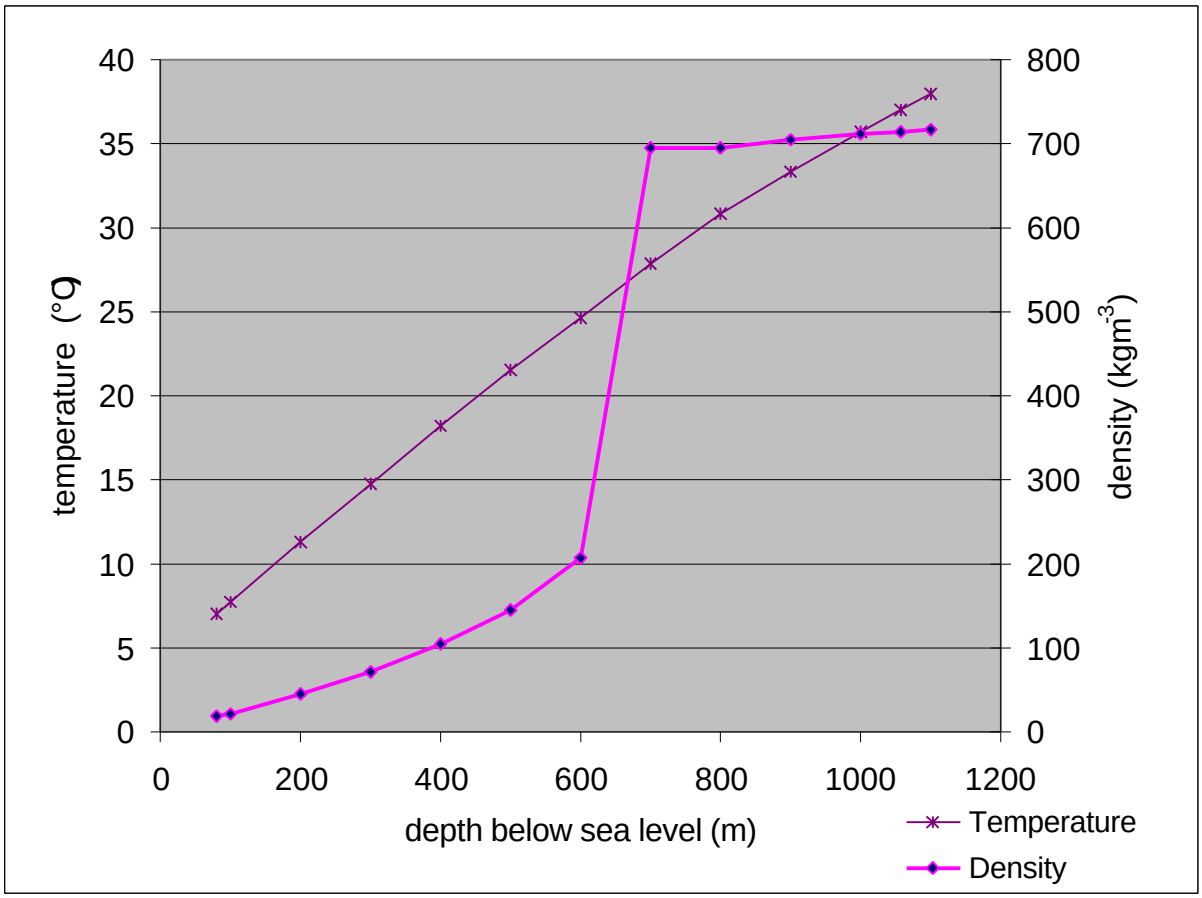

Figure 6 Temperature-depth and density-depth profiles through the Utsira Sand and overburden.

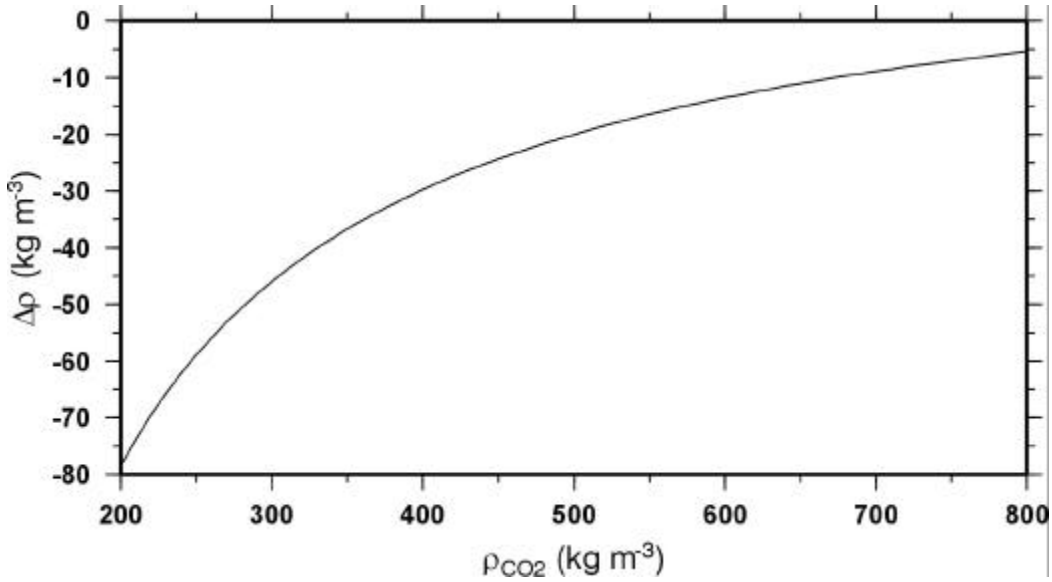

Figure 7 Effective density contrast of the bubble envelope volume as a function of CO_2 density.

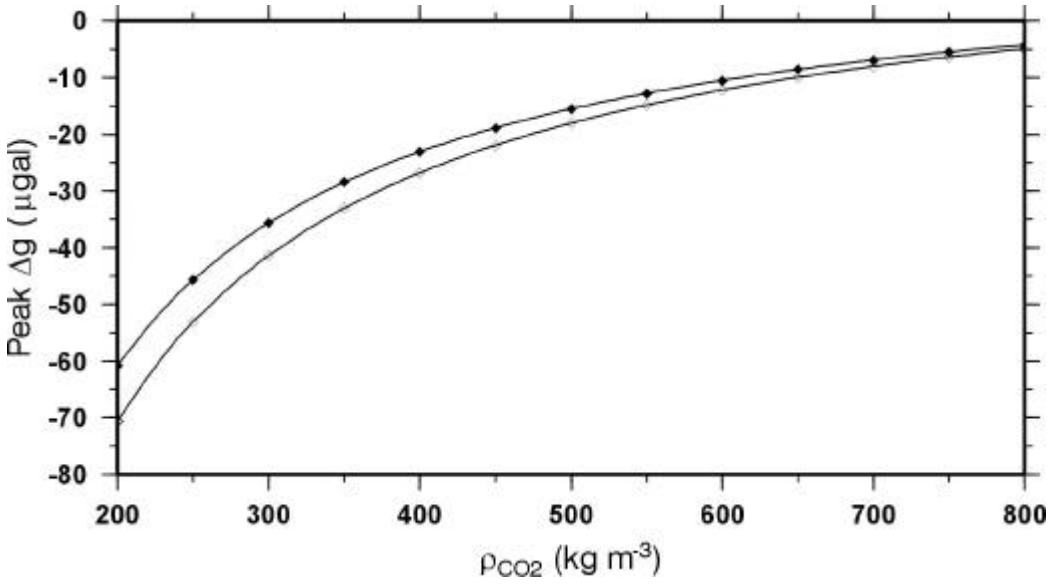

Figure 8: Peak gravity anomaly October 1999 due to the GOCAD model computed on the sea surface (solid symbols) and the sea bed (open symbols) as a function of CO_2 density.

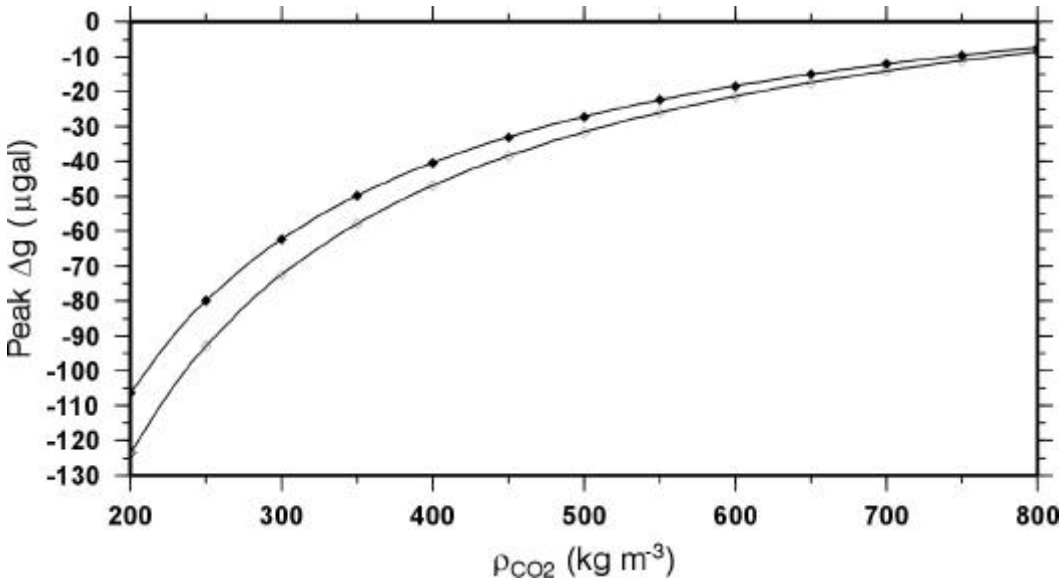

Figure 9: Peak gravity anomaly projected to 2001 (~ 4 MT CO_2) due to the GOCAD model computed on the sea surface (solid symbols) and the sea bed (open symbols) as a function of CO_2 density.

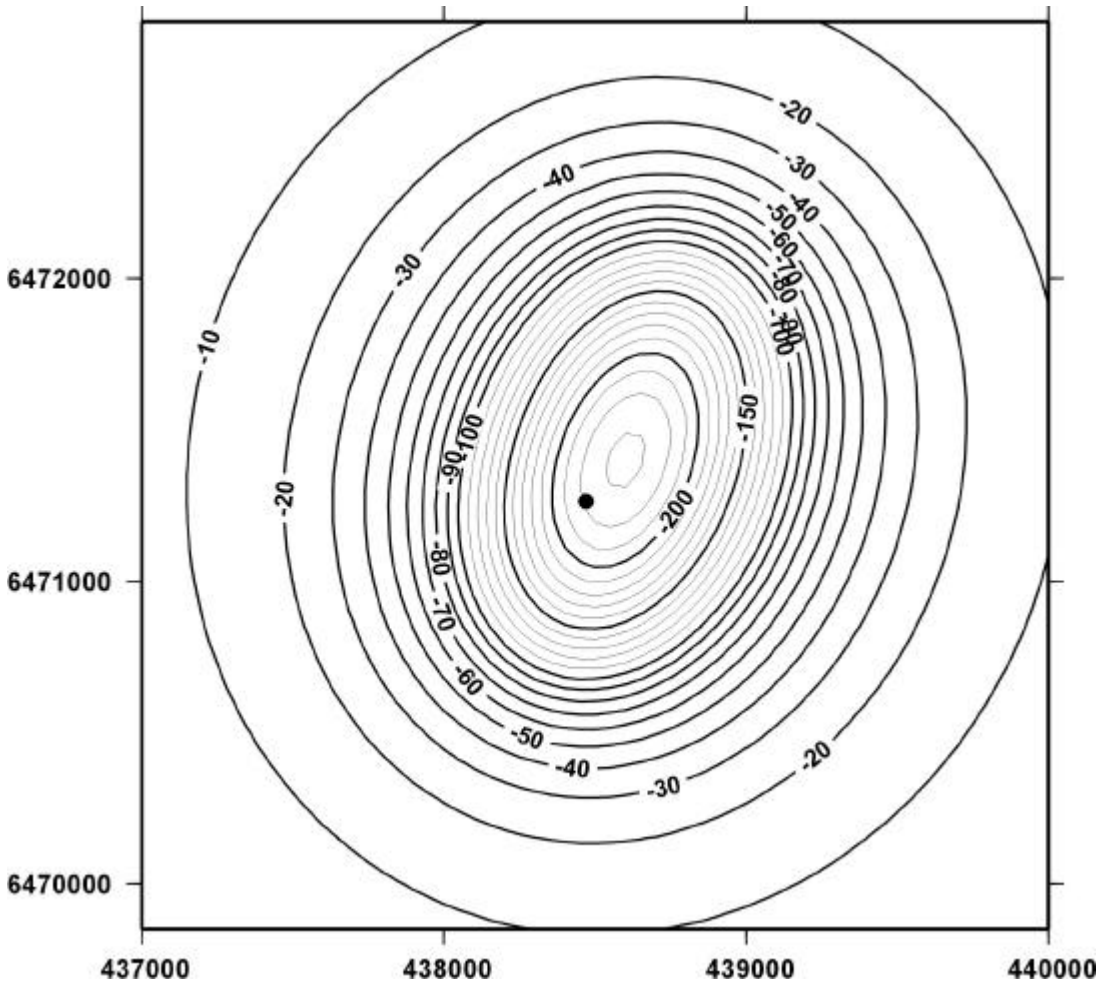

Figure 10. Modelled gravity anomaly for cylindrical approximation model, with top at 375 m depth and base at 600 m depth (ρ_{CO2} = 150 kgm^{-3}). Round marker denotes subsurface location of injection point.

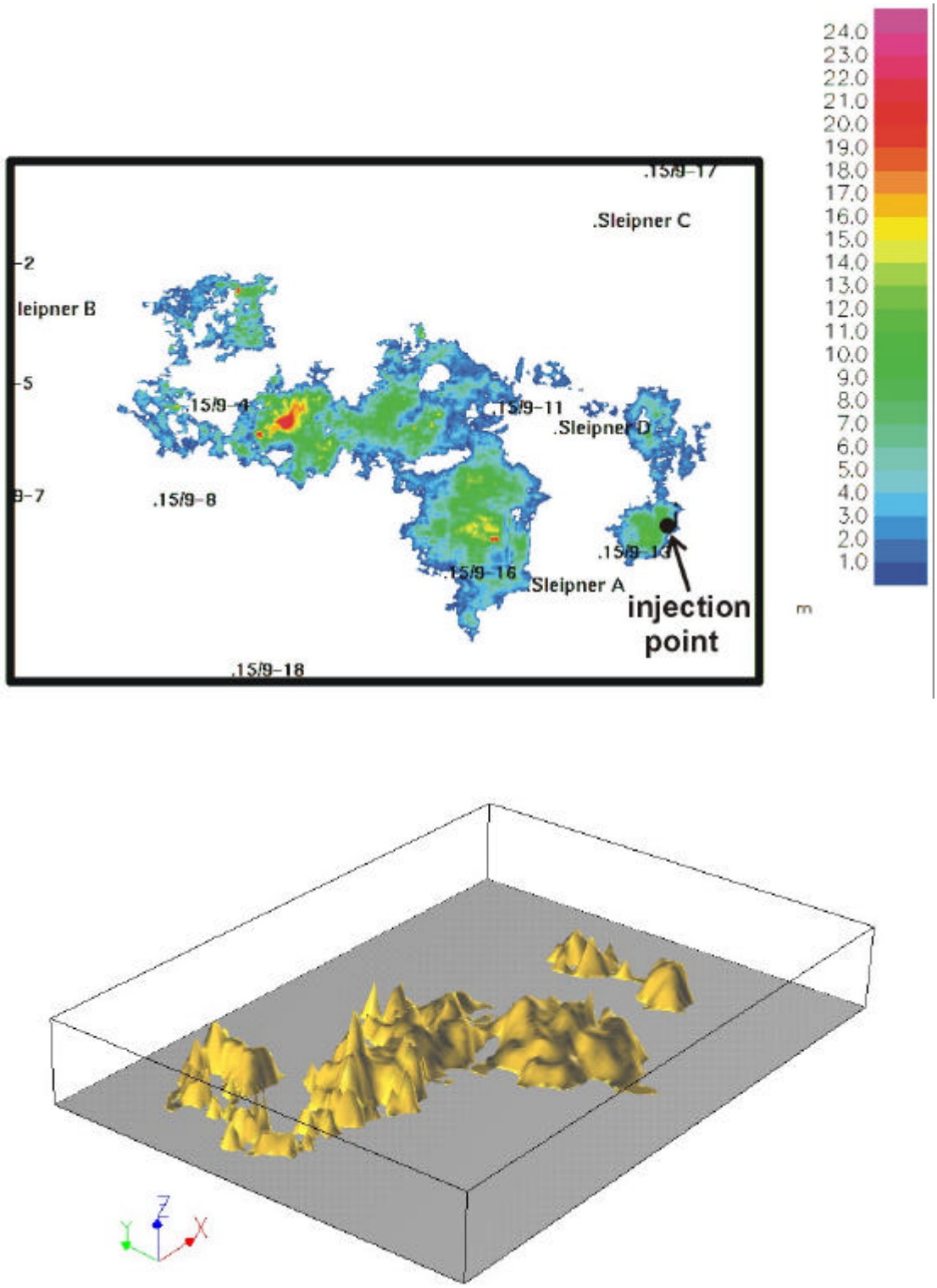

Figure 11 (a) Thickness of CO_2 saturated rock column after 21 MT of CO_2 injected, assuming CO_2 is trapped in structural closures at top Utsira Sand. Reservoir porosity = 0.3; net/gross = 0.85. From Zweigel et al. 2000. (b) Perspective view of the CO_2 accumulation viewed from the SW (vertical exaggeration x75).

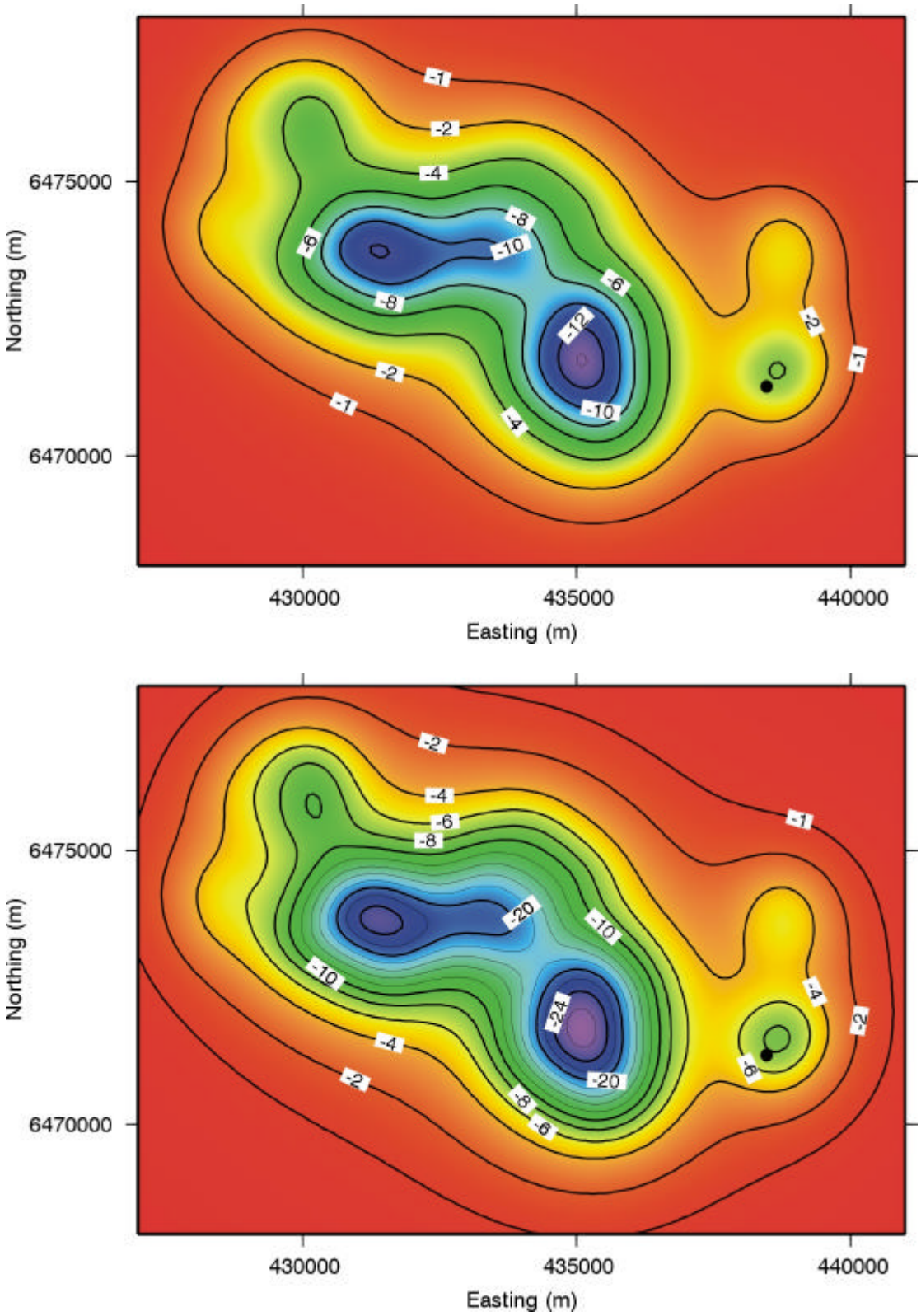

Figure 12 Modelled gravity anomalies (μGal) for 3 x 10^7 m^3 of injected CO_2 assuming lateral migration of a single thin layer of CO_2 beneath caprock (a) 21 MT at density of 700 kgm^3 (b) 10.5 MT at density of 350 kgm^3.